Vorticity and Divergence Fields within Tornadic Storms from Dual-Doppler Observations

PETER S. RAY

National Severe Storms Laboratory, NOAA, Norman, Okla. 73069

(Manuscript received 6 August 1975, in revised form 15 April 1976)

ABSTRACT

Tornadic storms passed between the two NSSL Doppler radars on 20 April and 8 June, 1974. Both radars simultaneously collected Dopplar data throughout these storms. From the derived velocity fields, vorticity and divergence calculations were made. Strongest convergence is noted in the weak echo region and between opposing vorticity centers.

1. Introduction

A recent paper by Ray *et al.* (1975) discussed dual-Doppler radar data obtained from a tornadic storm which passed between two National Severe Storms Laboratory (NSSL) radars on 20 April 1974. Three-dimensional velocity and reflectivity fields were presented from which the mesoscale circulation associated with the tornado was clearly apparent. Reflectivities in the storm exceeded $Z=10^6$ mm^6 m^{-3} which was consonant with reports of much hail. Maximum updrafts were northeast and maximum downdrafts southwest of the circulation center.

In the morning of 8 June 1974, a cold front extended across Oklahoma from NE to SW to a developing subsynoptic low in New Mexico. This was supported by a closed upper-level circulation over western Colorado which moved over Nebraska by the next day. The jet stream flowed from the Pacific, northwest through Arizona and Oklahoma, with winds exceeding 30 m s^{-1} at 500 mb. As the surface front occluded and moved into Oklahoma during the day, many tornadic storms developed and moved northeast, in association with a dryline over the Norman area.

The sounding shown in Fig. 1 was taken at Norman 2.5 h preceding the 8 June observations presented here. Although the saturation indicated below 2.5 km was probably due to passage through a cloud layer, copious available moisture enhanced the severe weather potential. The weak 600 mb inversion and the overlying nearly adiabatic layer suggests descending air from above this level. This concept is supported by a later sounding which showed an enhanced inversion closer to ground.

A storm emerged from the Norman radar's ground clutter about 1530 CST and shortly thereafter developed a reflectivity structure (hook echo) suggesting an intense circulation and possible tornado. This paper presents an analysis of data taken about midway during the tornado's contact with the ground. The tornado's damage path is indicated in Fig. 2 by the stippled arrow and the analysis grid is shown by the square which nearly encompasses the irregularly shaped common Doppler data area. Grid spacing is indicated by dots in the grid's lower right corner.

2. Analysis

Construction of velocity fields from dual-Doppler observations is facilitated if done in cylindrical coordi-

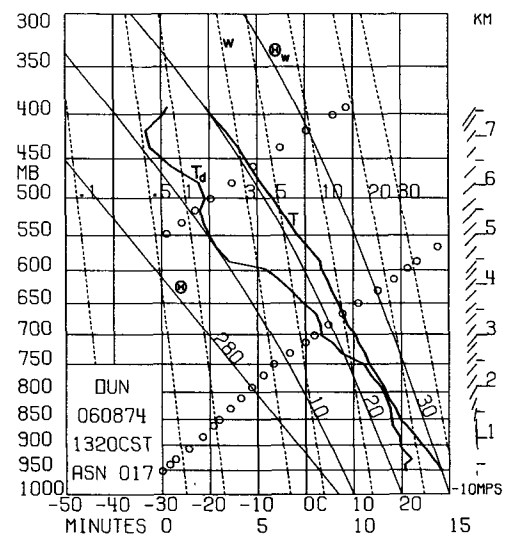

FIG. 1. Stüve diagram of sounding taken 2.5 h before data collection. Circles represent balloon ascent rate. Wind direction and magnitude are represented on the right, with north being vertical, and a 10 m s^{-1} magnitude scale is shown in the lower right corner.

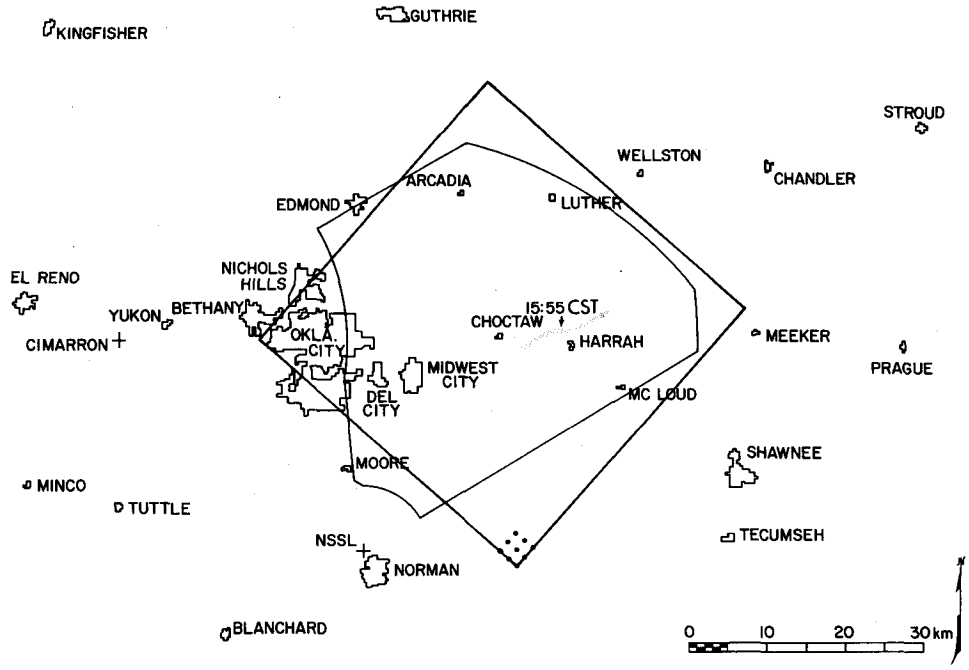

FIG. 2. Map of central Oklahoma showing the location of the two Doppler radars (Norman and Cimarron), the area of common Doppler coverage at 0° elevation, area of analysis, grid-point spacing (1.5 km) and tornado damage track (stippled arrow) for 8 June storm.

nates. The synthesized fields are then cast from a cylindrical to a Cartesian frame for convenience of interpretation. The analysis consists of:

1) Spatial interpolation of Doppler velocities to equally spaced grid points located on a series of planes which pass through the radar locations and are tilted at an angle α from horizontal.

2) Synthesis of Doppler velocities to derive two orthogonal cylindrical components in the plane through the two radars defined by constant elevation angle α.

3) Integration of the mass continuity equation to determine the velocity component normal to the α plane.

4) Interpolation to Cartesian coordinates.

Reflectivity fields, determined by distance weighting each radar's measured power, were used in an empirical terminal-velocity/reflectivity law to account for contribution of particle fallspeed to vertical velocity. Details of this analysis and characteristics of the Doppler radars are given in Ray *et al.* (1975).

Particular to this analysis were the choices of a spherical influence volume, used to compute grid values, of 1.5 km radius and the grid translation to ($x=-8$ km, $y=12$ km) where (0,0) is the mid-point on the line connecting the radars. Storm motion (13.6 m s^{-1} from 214.0°), estimated by correlating successive intensity scans at 0° elevation, was used to advect all measured quantities to their projected position at a time midway in data collection sequences. Although 4 min was required to complete the scan sequence, the maximum distance any data were advected (the top and bottom) was 1.6 km. It is presumed that the essential features of the storm were steady over the 4 min data acquisition time. The radar beams typically do not sample a common point simultaneously. However, the maximum time difference between their estimates is about 15 s, during which the storm translates only a fraction of a beamwidth.

3. Results

The radars sampled a common precipitation volume ($Z>10^2$) of 1.6×10^4 km^3, similar to that sampled 20 April. Reflectivity, wind (relative to the mean Doppler-derived wind at each altitude), horizontal divergence and vertical vorticity ($\zeta=\mathbf{k}\cdot\nabla\times\mathbf{V}$, where $\mathbf{k}$ is a unit vector in the z direction) are presented on planes parallel to the earth's surface in Figs. 3 and 4 (parts a and c). The mean Doppler-derived horizontal wind is indicated by a short arrow in the lower right corner. Thus, flow relative to the ground is simply the vector sum of the displayed velocity field and the indicated mean.

Streamlines have been drawn for illustration. As in the 20 April case, the vertical variation of mean wind is very similar to the environmental winds. This may be seen by comparing mean values with winds from the sounding (Fig. 1). The linear correlations from the product-moment for 20 April and 8 June are, respectively, 0.83 and 0.85 in direction and 0.82 and 0.68 for wind speed.

On the right side of the figures that illustrate reflectivity, chaff is evident at 1 and 3 km. This experiment, described by McCarthy and Heymsfield (1974), involved distributing chaff in a series of 2600 m deep columns from an airplane which simultaneously collected data on wind and thermodynamic variables. No velocity field could be determined in this region as the prescribed azimuthal scan limit for each radar allowed only one Doppler radar to illuminate the chaff-filled volume at this time. Maximum reflectivities, nearly 10 dBZ lower than those for 20 April, were consistent with smaller size and amounts of hail produced by this storm.

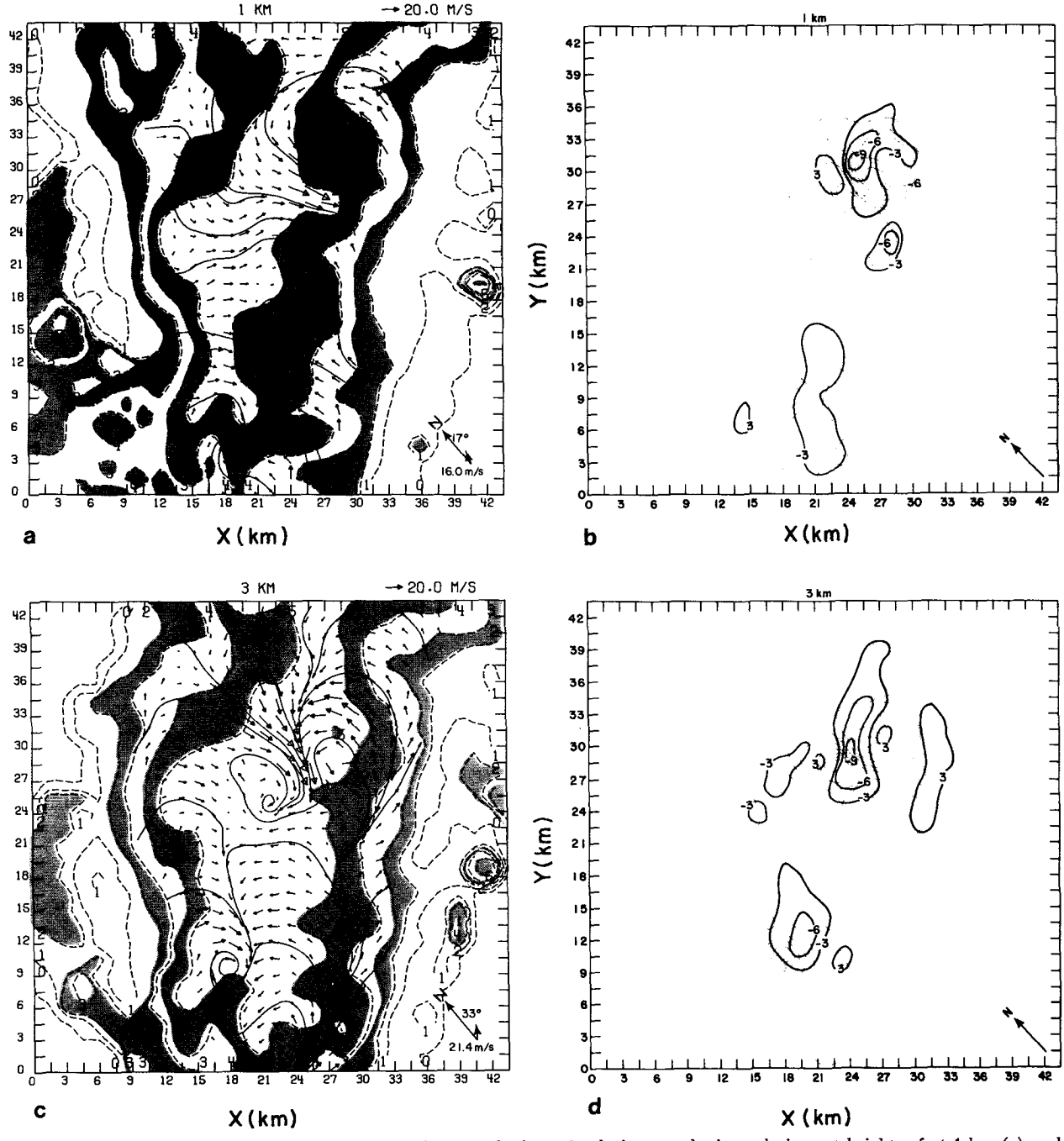

FIG. 3. Log-reflectivity field and deviation from the mean horizontal velocity on a horizontal plane at heights of at 1 km (a) and 3 km (c) for the 8 June storm. Alternate reflectivity levels are shaded for clarity. Coordinate origins are at $x=-10$, $y=+15$. Arrow next to the north vector indicates mean wind at that level. Vertical vorticity ($\times 10^{-3}$ s^{-1}) is indicated in (b) and (d) by grey lines and horizontal divergence ($\times 10^{-3}$ s^{-1}) by black lines.

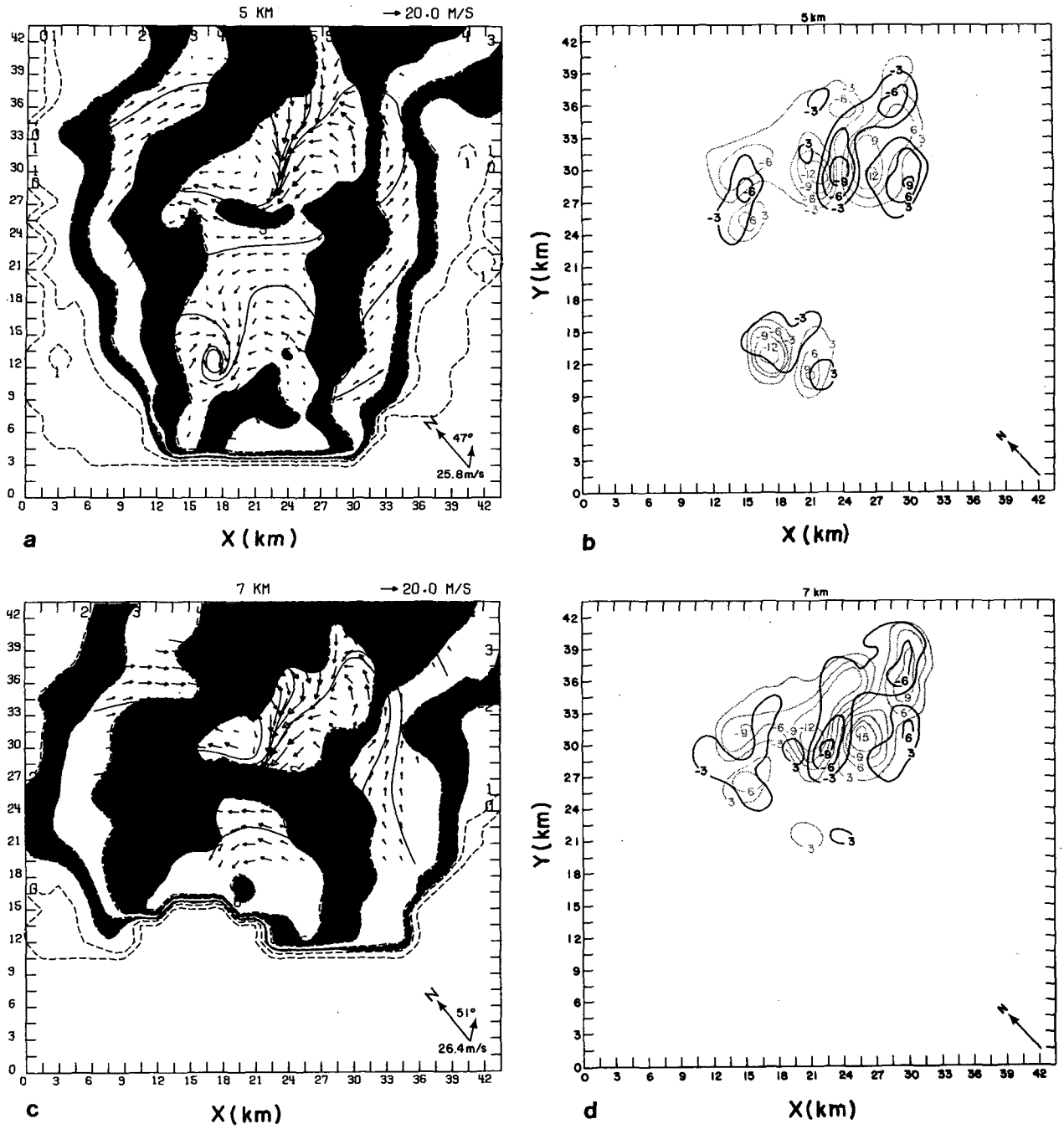

FIG. 4. As in Fig. 3 except at heights of 5 km (a) and 7 km (b). Coordinate origins are at $x=-10$, $y=+15$.

Several regions of cyclonic and anticyclonic circulation as well as a strong convergence line are verified in Figs. 3b,d and 4b,d. Here, solid black lines represent isopleths of horizontal divergence and grey lines isopleths of the vertical component of vorticity. Thus, there are regions where the vorticity exceeds 1.8×10^{-2} s^{-1} and where convergence is near 10^{-2} s^{-1}.

A gust front evident in Fig. 3 and verified by subsequent Doppler data and an associated convergence area extend southwest of the circulation. An apparent gust front was also found in the 20 April storm where it tilted to the north with height, as illustrated in the convergence field in Fig. 5.

Eight vertical cross sections through the most intense circulation region of the 8 June storm depicts reflectivities and wind (relative to the mean horizontal wind in each portrayed plane) shown in Figs. 6 and 7. Planes are for increasing y in the first figure and for decreasing

x in the second. Each plane's coordinate is labeled at the top of each cross section. The upper boundary reflects the maximum radar antenna elevation angle during data collection rather than maximum storm height.

A strong downdraft was found southwest of the circulation center in the 20 April case. In the 8 June case, only a weak downdraft was evident at that location. Strong convergence indicated in Figs. 6 and 7 is confirmed in Figs. 8 and 9, respectively. The forward edge of Figs. 4a and 4c is due to the elevation limits of the tilt sequence and is thus an artificial boundary. The convergent area is between areas of opposing vorticity throughout the depth of collected data. Maximum vorticity on 20 April is associated with a nondivergence level (5 km) as evidenced in Figs. 10 and 11. For 8 June, maximum computed vorticity exceeded 1.8×10^{-2}

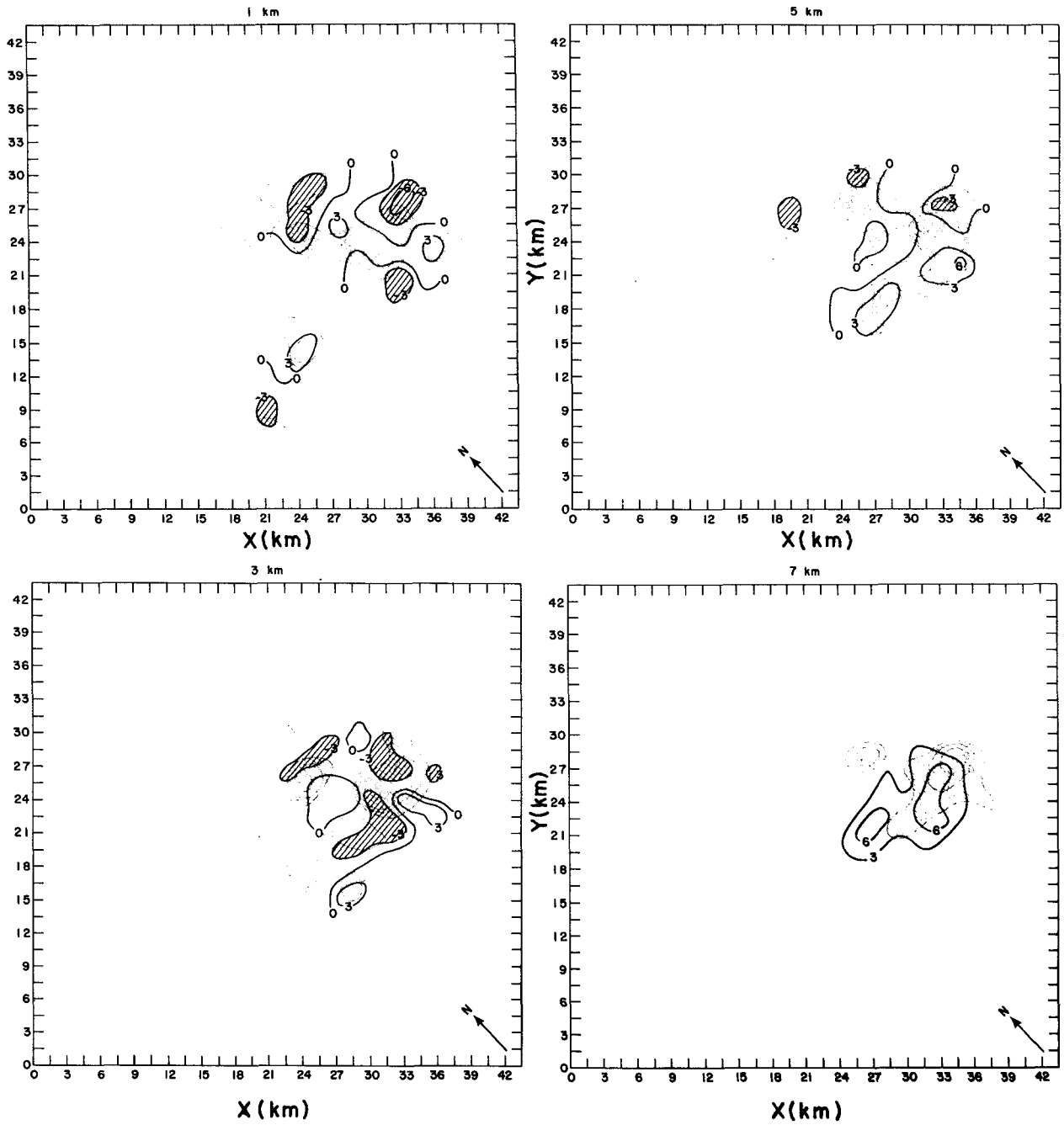

FIG. 5. Vertical vorticity ($\times10^{-3}$ s^{-1}) at four levels on 20 April 1974 indicated by grey lines and horizontal divergence ($\times10^{-3}$ s^{-1}) by black lines.

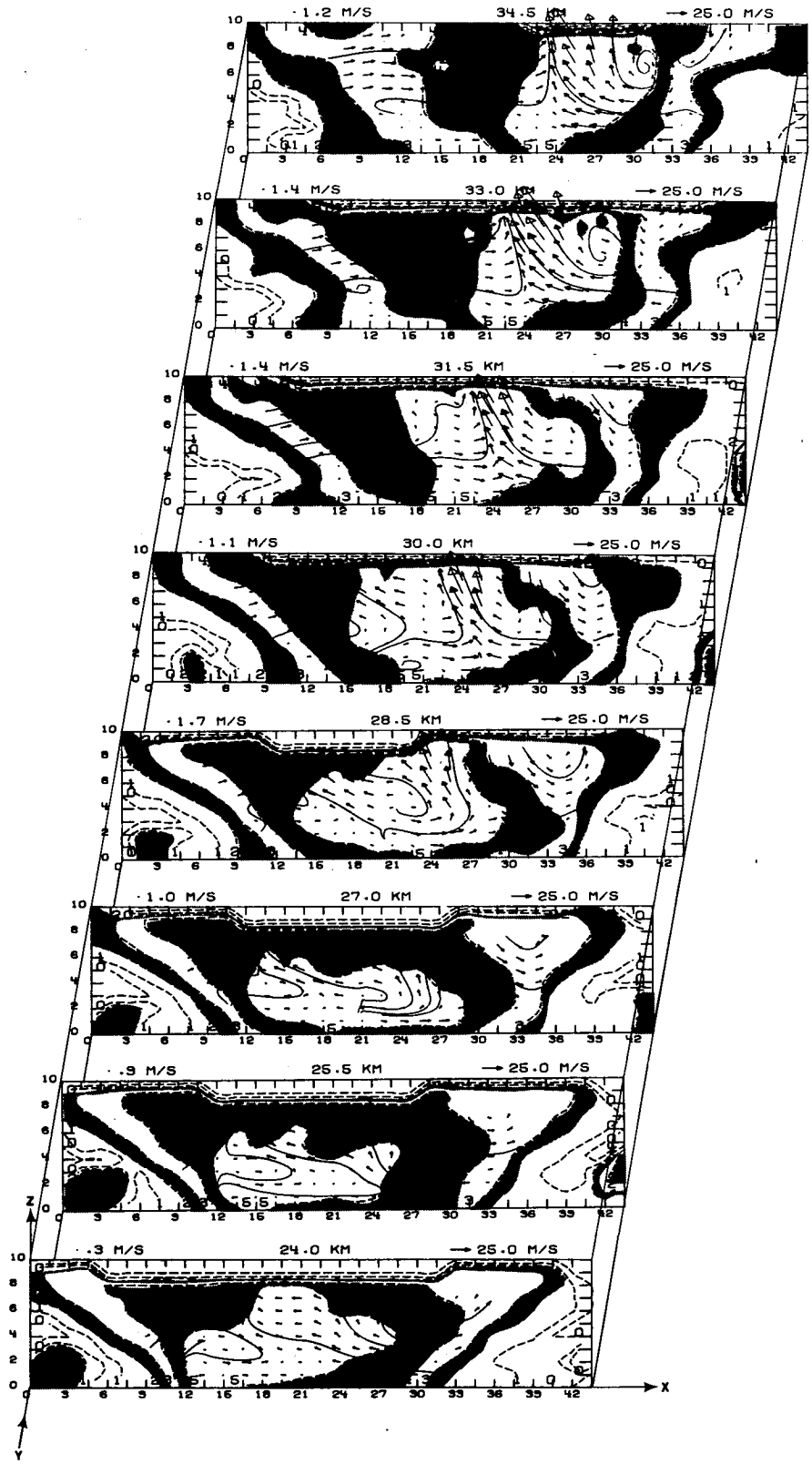

FIG. 6. Reflectivity and velocity field in the x-y plane for eight planes for increasing values of y. The mean horizontal velocity in each vertical plane was removed and is indicated in the upper left of each plane.

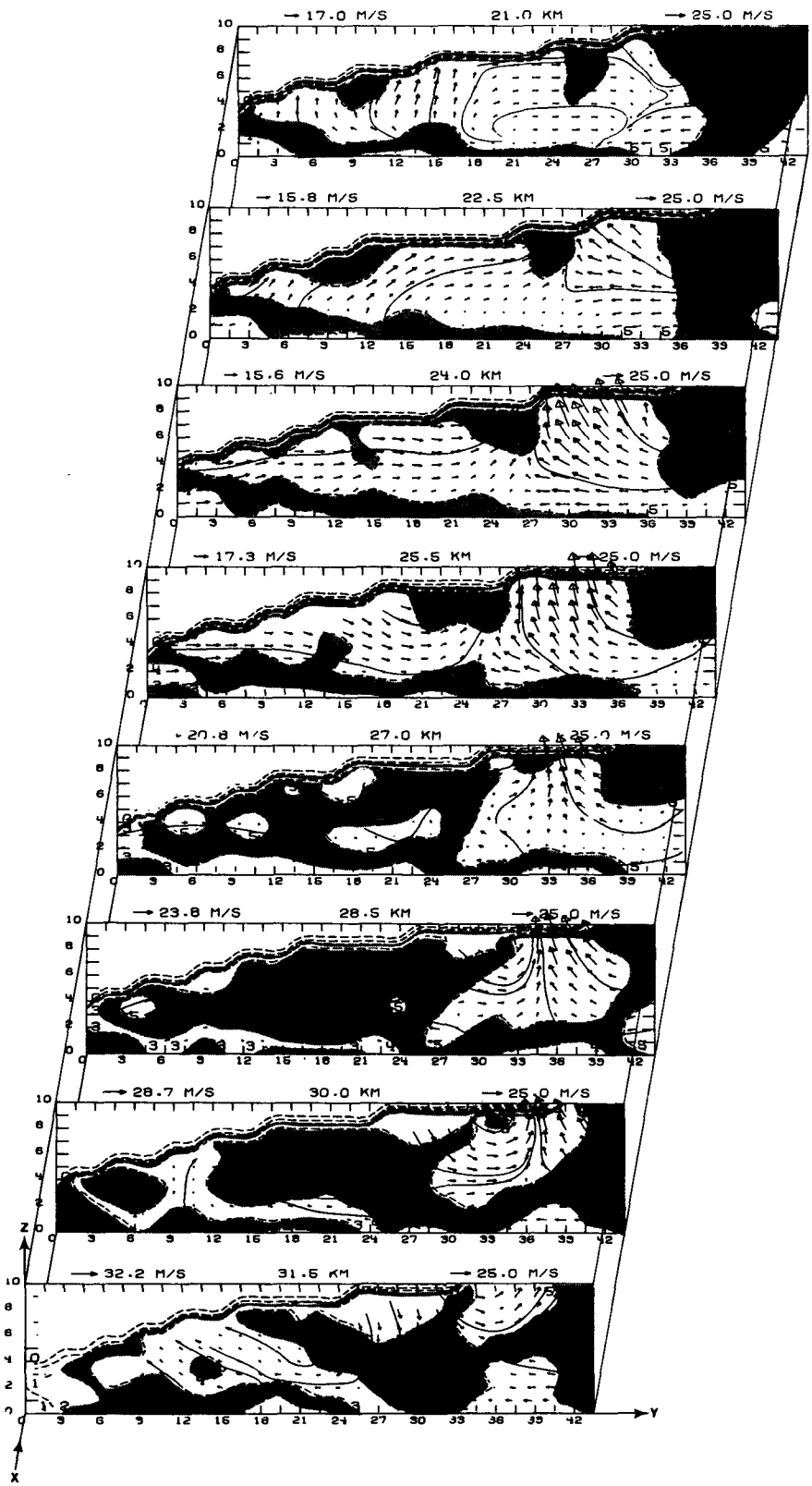

FIG. 7. As in Fig. 6 for decreasing values of x in the y-z plane.

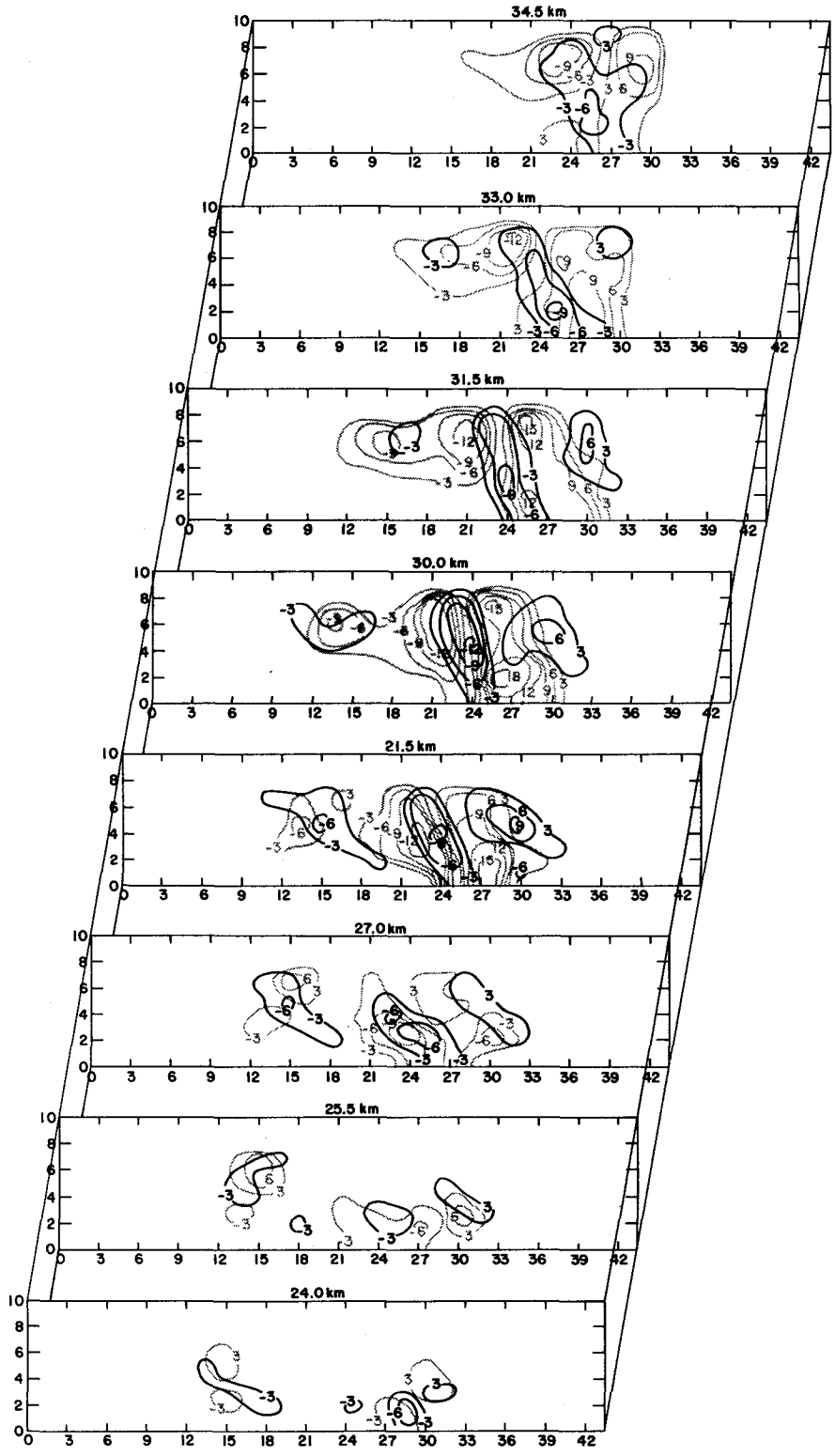

FIG. 8. Vorticity and divergence fields in eight x-y planes for 8 June 1974 for increasing values of y. Vorticity is indicated by grey lines and divergence by solid black. Both are times 10^{-3} s^{-1}.

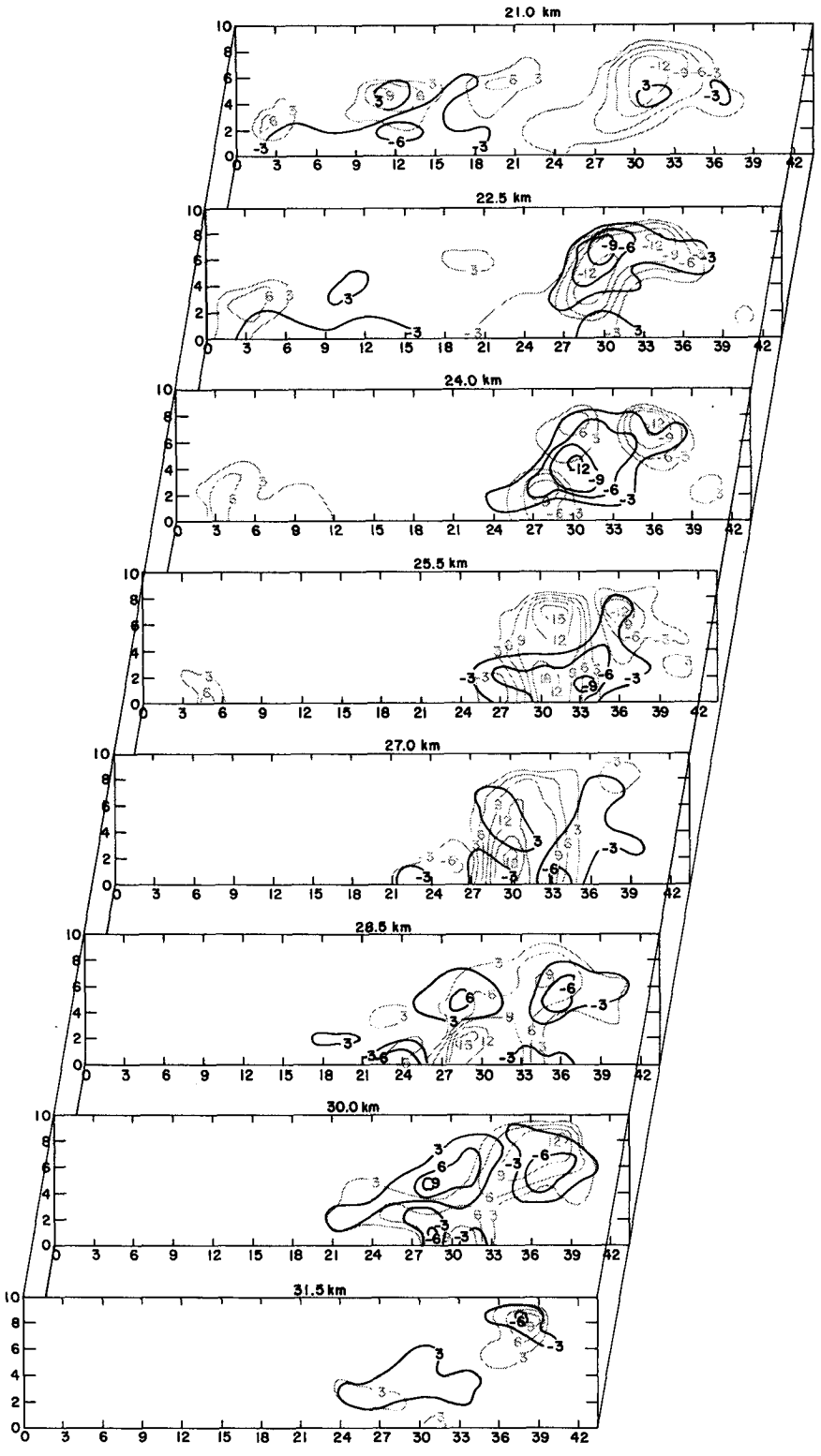

FIG. 9. As in Fig. 8 except in y-z planes.

s^{-1} and was centered about 1 km north of the tornado ground track. In fact, the vorticity is still appreciable near the top of the data region (see Fig. 4). The contrary impression given in Figs. 8 and 9 is an artifact of the contouring routine. Other aspects of these fields are discussed below.

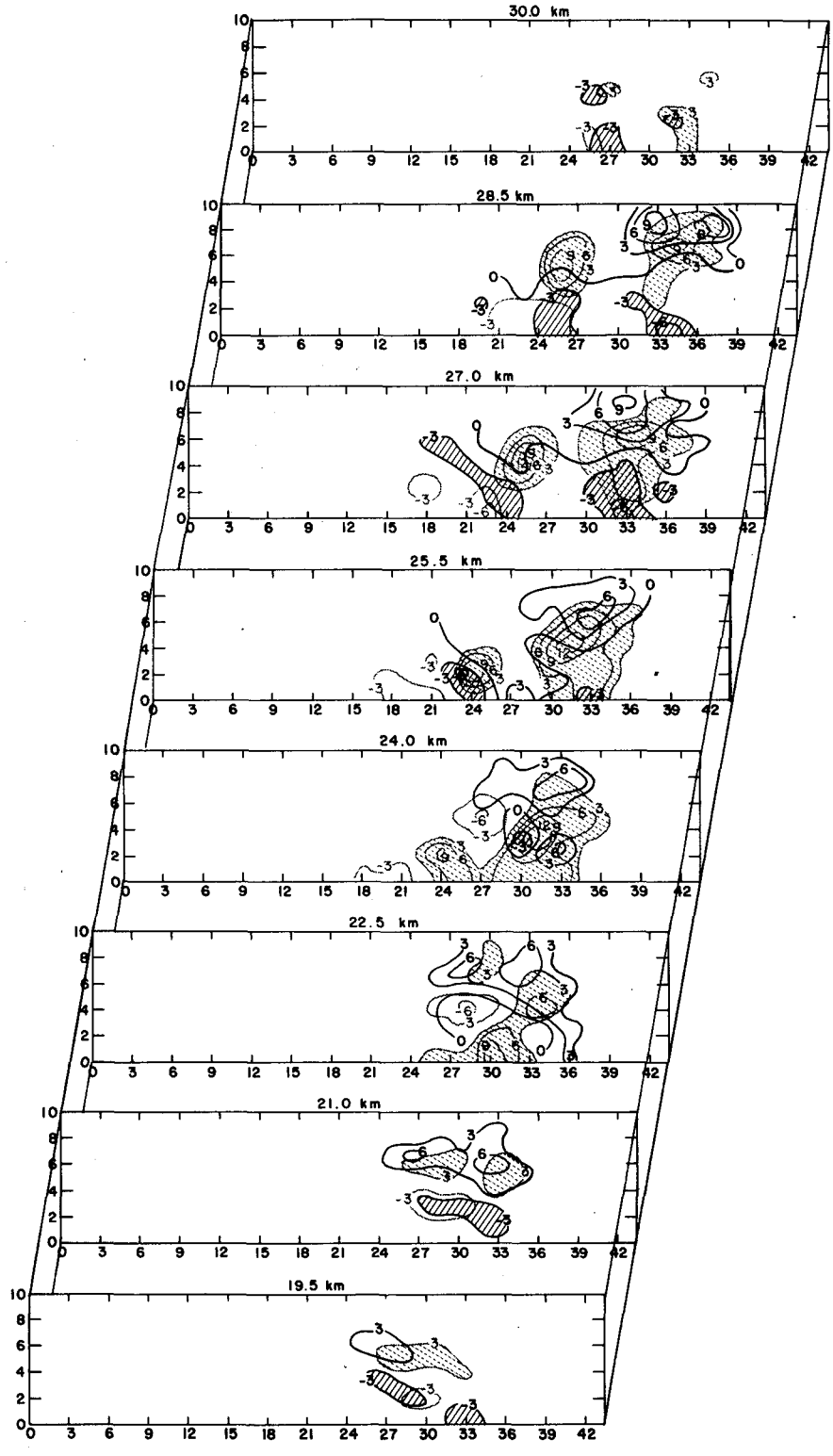

FIG. 10. As in Fig. 8 except for 20 April 1974.

4. Discussion

Relative to the ground, and to a lesser extent relative to the storm motion vector, interior storm winds appear to flow around regions of strong convergence, which may be interpreted as updrafts. This is a consistent picture, as shear over the differencing interval would yield the calculated vorticity and an updraft scale greater than the grid spacing would produce a pair of

vorticies of opposite sign. The interpretation is perspective-dependent.

Mention should be made of the uncertainty in vertical velocity estimates. In addition to uncertainty introduced in integration, uncertainty in the lower boundary is critical. Divergence may be a maximum in the lowest few hundred meters where it may be poorly sampled or undetected by radar. This is due to ground clutter,

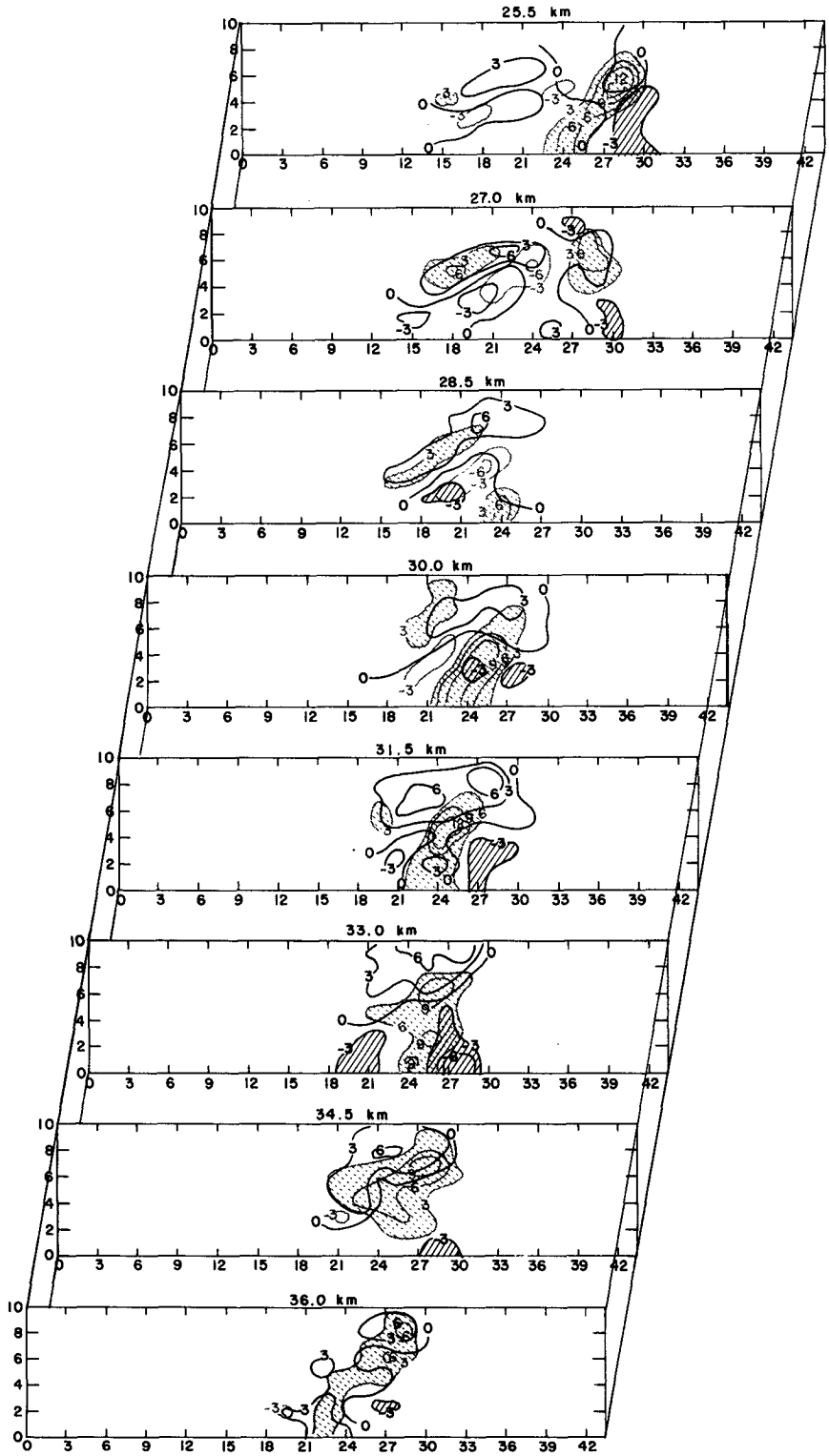

FIG. 11. As in Fig. 8 except for 20 April 1974 and in the y-z plane.

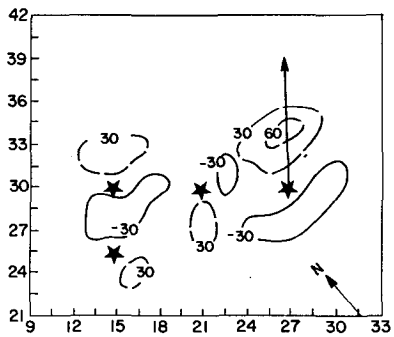

FIG. 12. Local vorticity (10^{-6} s^{-2}) change for 8 June. Broken lines represent areas of increasing positive vorticity, the stars vorticity centers.

blockage, possible lack of scatterers and earth curvature effects. This introduces a nearly constant bias in vertical wind estimates throughout the storm depth. However, the bias is horizontally variable. Thus, it is difficult to estimate their uncertainty. The horizontal winds are determined to within a few tenths of a meter per second, which was consonant with the noise level in the vorticity-divergence calculations. Vertical velocities obtained in this manner must be viewed with caution, e.g., the gust front formation is related to a downdraft and subsequent outflow. Yet, in the gust front region only a weak downward component exists in this analysis, probably due to inadequate estimates of large divergence in a relatively shallow layer. This problem may be ameliorated by an independent estimate of vertical velocity such as might be provided by additional radars or locally by aircraft penetrations, etc., or by appropriate constraining relations.

The local vertical vorticity change is

$$\frac{\partial \zeta}{\partial t} = -\mathbf{V}_h \cdot \nabla (f+\zeta) - w\frac{\partial \zeta}{\partial z} - (f+\zeta)\nabla \cdot \mathbf{V}_h - \frac{2\Omega \cos\phi}{a} v$$
$$-\left(\frac{\partial w}{\partial x}\frac{\partial v}{\partial z} - \frac{\partial w}{\partial y}\frac{\partial u}{\partial z}\right) + \left(\frac{\partial P}{\partial x}\frac{\partial \alpha}{\partial y} - \frac{\partial P}{\partial y}\frac{\partial \alpha}{\partial x}\right), \quad (2)$$

where P is pressure, α specific volume, f the Coriolis parameter, Ω the angular velocity of the earth's rotation, and a the earth's radius. The $2\Omega(v/a)\cos\phi$ term is of order 10^{-10} and may be neglected as may f compared to ζ. The last term, the so-called "solenoidal term," does not appear in an anelastic system which is one of the analysis assumptions used here as well as in most numerical cloud models. This term is also zero in a axisymmetric circulation (mesovortex). In the worst case envisionable, with the pressure and density contours orthogonal in a horizontal plane and with horizontal pressure and temperature gradients of 1 mb km^{-1} and 10°C km^{-1}, respectively, this term would be on the order of 4×10^{-6} s^{-2}. In practice one might expect it to be much smaller.

A more comprehensive dual-Doppler error analysis is in preparation, but an examination of the fields indicates the noise level of the computation to be about 10^{-6} s^{-2}.

The local change in vorticity is given in Fig. 12 with the stars representing the vorticity center locations. The estimated storm motion is indicated by the arrow originating from the strongest vorticity center. The estimated translation speed based on the vorticity change ($\sim$40 m s^{-1}) is an overestimate, but of the correct order. The local change is due to advection and forcing terms. At this time the advective term is about four times larger and dominates the forcing terms (the so-called "tilting" and "stretching" terms) centered east of the vorticity centers. This is expected as these data were taken near the time the storm was most nearly in a relative steady state. It is further confirmed by estimating $D\zeta/Dt$ using a subsequent analysis. Assessing the role of these terms early in the storms' evolution will lend insight into rotation sources, generation and intensification of vorticity centers, and ultimately to tornado formation itself.

Acknowledgments. Dr. Robert Davies-Jones' (NSSL) insight through illuminating conversations are gratefully acknowledged. Acknowledgment is also made to a reviewer's constructive comments and to Dr. G. L. Achtemeier of Illinois State Water Survey for his contribution in developing the contour and streamline plotting subroutines. These experiments were made possible in part through support of the Federal Aviation Agency for development of the radar sensors under Interagency Agreement DOT-FA72-WAI-265, and through support of the Atomic Energy Commission under Interagency Agreement AT(49-5)1289.

REFERENCES

McCarthy, J., and G. M. Heymsfield, 1974: Experiment to deduce tornado cyclone inflow characteristics using chaff and NSSL dual-Doppler radars. *Bull. Amer. Meteor. Soc.*, **55**, 1130–1131.

Ray, P. S., R. J., Doviak, G. B. Walker, D. Sirmans, J. Carter and B. Bumgarner, 1975: Dual-Doppler observations of a tornadic storm. *J. Appl. Meteor.*, **14**, 1521–1530.